



# Theoretical and experimental studies of a bi-metallic heat switch for space applications

Fernando H. Milanez<sup>\*</sup>, Marcia B.H. Mantelli

*Satellite Thermal Control Group, Department of Mechanical Engineering, Federal University of Santa Catarina, P.O. Box 476, 88040-900 Florianopolis, SC, Brazil*

Received 17 July 2002; received in revised form 10 June 2003

## Abstract

This work presents theoretical and experimental studies on a passively actuated bi-metallic heat switch for space applications. The working principle of the heat switch is based on the differential thermal expansion of distinct metals. Analytical one-dimensional and two-dimensional heat conduction models are developed to predict the thermal resistance of the heat switch, which is a function of temperature. A non-dimensional parametric analysis is performed in order to study how the design parameters affect the total thermal resistance of the heat switch. The theoretical models are also compared with experimental data obtained from a prototype of the heat switch. The agreement between theory and experiments is good.

© 2003 Elsevier Ltd. All rights reserved.

## 1. Introduction

Heat switches are devices that present variable thermal resistance. Many different heat switch configurations have been developed for spacecraft applications over the last three decades [1–5]. Each configuration is based on a different working principle, but all of them were developed for applications in cryogenic systems of satellites. The heat switches proposed by Frank and Nast [1], Nast et al. [2], Naes and Nast [3] and Van Oost et al. [4] were developed to couple radiation sensors to cryogenic refrigerators. When the radiation sensor is operating, it is necessary a low thermal resistance between the sensor and the refrigerator in order to keep the sensor temperature as low as possible. In this situation, the heat switch provides a good thermal coupling between the radiation sensor and the cryogenic refrigerator. However, sometimes it is convenient to disconnect the sensor from the refrigerator, as for example in re-

dundant refrigeration systems, in order to avoid parasitic heat loads coming from refrigerators turned off. Under these circumstances, the heat switch must provide a high thermal resistance between the sensor and the deactivated refrigerator.

The gas-gap type heat switches proposed by Frank and Nast [1] and by Nast et al. [2] are similar. They consist basically of two cylindrical pieces separated by a small gap, which is filled with a conductive gas. The thermal resistance between the two cylindrical pieces is a function of the amount of gas that fills the gap. These heat switches are actively actuated, i.e., they require external energy to operate.

The heat switches proposed by Naes and Nast [3], by Van Oost et al. [4], and by Milanez and Mantelli [5] are based on the differential thermal expansion of distinct metals. Although based on the same working principle, these configurations are quite different from each other. The bi-metallic heat switches are passively actuated, that is, they do not require external energy to operate, and the thermal resistance is function of the mean temperature level of the heat switch. The heat switches of Naes and Nast [3] and Van Oost et al. [4] were also developed to couple radiation sensors to cryogenic refrigerators in redundant systems.

<sup>\*</sup> Corresponding author. Tel.: +55-48-234-2161x226; fax: +55-48-331-7615.

E-mail addresses: [milanez@labsolar.ufsc.br](mailto:milanez@labsolar.ufsc.br) (F.H. Milanez), [marcia@labsolar.ufsc.br](mailto:marcia@labsolar.ufsc.br) (M.B.H. Mantelli).



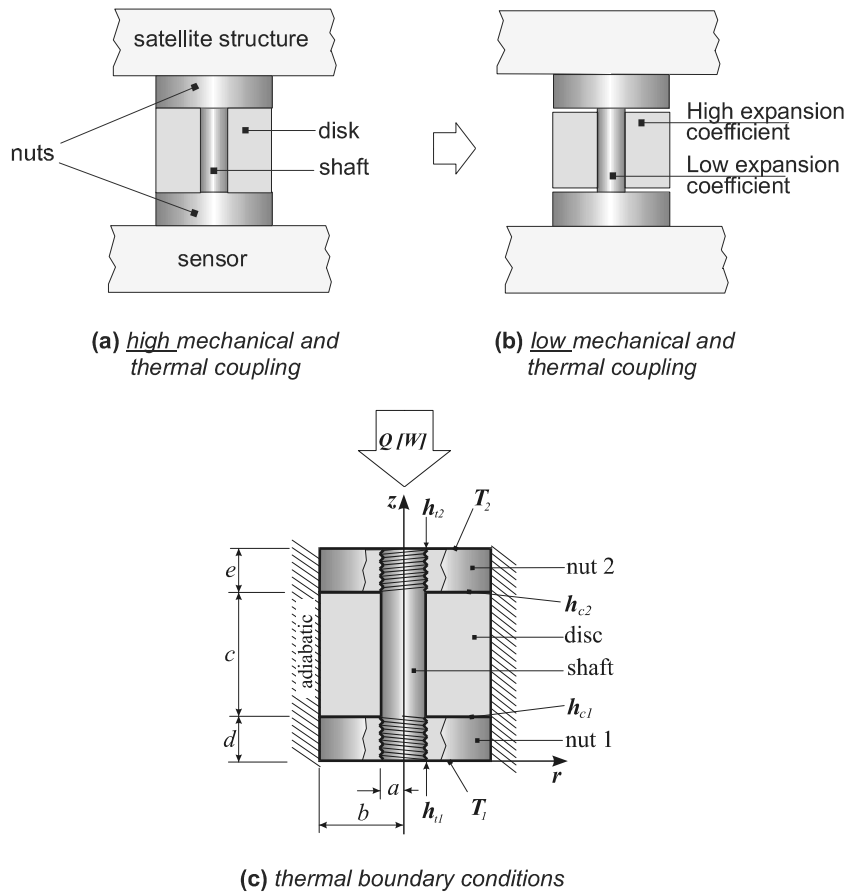


Fig. 1. Working principle (a and b) and thermal boundary conditions (c) of the heat switch.

theoretical model so that a design methodology can be established, and to compare the theoretical models with experimental data obtained from a prototype developed in the laboratory.

## 2. Thermal modelling

Fig. 1(c) shows a schematic of the geometry and the boundary conditions of the problem. The heat switch has a cylindrical shape, with an external radius  $b$ . The radius of the shaft is  $a$ . The thicknesses of the nut 1, disk and nut 2 are  $d$ ,  $c$  and  $e$ , respectively. A heat load  $Q$  comes from the satellite structure and crosses the heat switch. At  $z = 0$  the heat switch is assumed to be at a uniform temperature  $T_1$ , which corresponds to the cryogenic sensor operation temperature. At  $z = c + d + e$ , the temperature is also assumed to be uniform and equal to  $T_2$ , which corresponds to the temperature of the satellite structure. The lateral walls, at  $r = b$ , are assumed to be adiabatic, because there is no convection heat transfer in vacuum environment and the heat

switch can be wrapped in multilayer insulation blankets (MLI) to avoid radiation heat transfer. The inner radius of the disk is slightly larger than the outer radius of the shaft so the thermal contact between the two elements is ineffective, that is, heat transfer is negligible between the two.

The contact conductances between the disk and the nut 1 and between the disk and the nut 2 are  $h_{c1}$  and  $h_{c2}$ , respectively. These conductances are assumed to be uniform in the interfaces. The thread contact conductances of nuts 1 and 2 are  $h_{t1}$  and  $h_{t2}$ , respectively. These contacts are assumed to be cylindrical, because the dimensions of the thread are much smaller than the diameter of the shaft. The thread contact conductances are also assumed to be uniform along the thread.

In the next two subsections, two analytical models are developed to predict the total thermal resistance as a function of the mean temperature of the heat switch: a two-dimensional model and a one-dimensional model. The total thermal resistance  $R_t$  and the mean temperature  $T_m$  of the heat switch are defined, respectively, as:

$$R_t = \frac{T_2 - T_1}{Q} \tag{1}$$

$$T_m = \frac{T_2 + T_1}{2} \tag{2}$$

2.1. Two-dimensional heat conduction model

For the development of the two-dimensional heat conduction model, it is assumed that the heat flow in the shaft and the disk ( $d < z < d + c$ ) is one-dimensional in the  $z$ -axis. In the nuts and in the shaft tips ( $z < d$  and  $z > d + c$ ) the heat flow is two-dimensional. Fig. 2(a) and (b) shows the thermal models adopted for the nuts and the shaft tips. The temperature fields are:  $\Theta(r, z)$  in the nut 1,  $T(r, z)$  in the tip 1,  $\beta(r, z)$  in the tip 2 and  $\xi(r, z)$  in the nut 2. The one-dimensional heat fluxes crossing the shaft and the disk are  $q_s$  and  $q_d$ , respectively. To solve this problem, we have to find the coupled temperature fields  $\Theta(r, z)$ ,  $T(r, z)$ ,  $\beta(r, z)$ ,  $\xi(r, z)$ . Knowing

these temperature fields one obtains the total temperature drop across the heat switch ( $T_2 - T_1$ ) (Eq. (1)). In steady-state, the temperature fields are obtained by solving Laplace's equation. Due to the symmetry of the problem, Laplace's equation is given by:

$$\frac{1}{r} \frac{\partial}{\partial r} \left( r \frac{\partial T}{\partial r} \right) + \frac{\partial^2 T}{\partial z^2} = 0 \tag{3}$$

The temperature fields of the tip 1 and of the nut 1 are obtained by solving the equation above subjected to the following boundary conditions (see Fig. 2(a)):

$$\begin{cases} k_s \frac{\partial T}{\partial z} = q_s & 0 < r < a \\ k_{n1} \frac{\partial \Theta}{\partial z} = q_d & a < r < b \end{cases} \text{ at } z = d \tag{4}$$

$$T = \Theta = T_1 \text{ at } z = 0 \tag{5}$$

$$\frac{\partial T}{\partial r} = 0 \text{ at } r = 0 \tag{6}$$

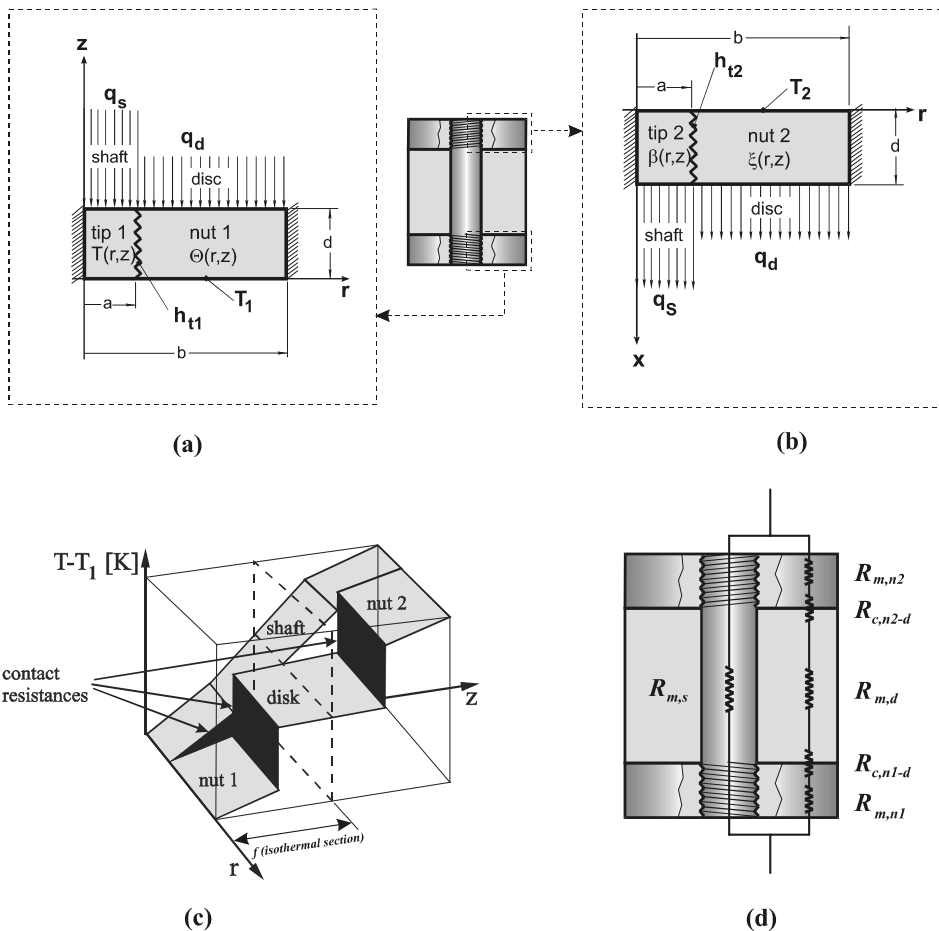


Fig. 2. Thermal models: two-dimensional (a, b and c) and one-dimensional (d).

$$\begin{cases} k_s \frac{\partial T}{\partial r} = k_{n1} \frac{\partial \Theta}{\partial r} \\ -k_s \frac{\partial T}{\partial r} = h_{t1}(T - \Theta) \end{cases} \quad \text{at } r = a \quad (7)$$

$$\frac{\partial \Theta}{\partial r} = 0 \quad \text{at } r = b \quad (8)$$

Using the method of separation of variables [6], one obtains the expressions for the two temperature fields as a function of  $q_s$  and  $q_d$ . Table 1 shows the resulting expressions for the temperature fields of the tip 1 (Eq. (9)) and the nut 1 (Eq. (10)).

The next step is to compute  $q_s$  and  $q_d$ , the heat fluxes crossing the shaft and the disk which are still unknown. A sketch of the temperature field of the heat switch is shown in Fig. 2(c). At  $z = f$ , named here the isothermal section, the temperature of the disk is equal to the temperature of the shaft. Mathematically, this can be written as:

$$\begin{aligned} \frac{2}{a^2} \int_0^a T(r, d)r dr + q_s \frac{f-d}{k_s} \\ = \frac{2}{(b^2 - a^2)} \int_a^b \Theta(r, d)r dr + q_d \frac{1}{h_{c1}} + q_d \frac{f-d}{k_d} \end{aligned} \quad (12)$$

where  $T(r, d)$  and  $\Theta(r, d)$  are obtained substituting  $z = d$  into Eqs. (9) and (10) of Table 1, respectively. The left hand side of the expression above is the temperature of the shaft, and the right hand side is the temperature of the disk, both at  $z = f$ . The first term in the left hand is the mean temperature of the tip 1 at  $z = d$ , and the second term is the temperature drop in the shaft between  $z = f$  and  $z = d$ . Similarly, the first term in the right hand side is the mean temperature of the nut 1 at  $z = d$ , the second term is the temperature drop due to the thermal contact resistance between the disk and the nut 1, and the third term is the temperature drop in the disk between  $z = f$  and  $z = d$ .

The energy conservation principle requires that:

$$q_s \pi a^2 + q_d \pi (b^2 - a^2) = Q \quad (13)$$

Solving Eq. (13) for  $q_s$ , substituting the resulting expression into Eq. (12), and solving for  $q_d$ , one obtains the expression for the heat flux across the disk  $q_d$  as a function of the isothermal section  $f$ , which is given by Eq. (14) of Table 1.

To compute  $f$ , the isothermal section, a similar procedure can be employed to find the temperature fields of the nut 2 and of the tip 2 (Fig. 2(b)). In this figure, a new coordinate system ( $x$ -axis) is defined for convenience, where:

$$x = c + d + e - z \quad (16)$$

Comparing Fig. 2(a) and (b), one can see that the models are similar. The temperature fields of the tip 2

and nut 2 are obtained by following the same procedure employed to obtain the temperature fields of the nut 1 and of the tip 1 (Eqs. (9) and (10), respectively). The expressions for the temperature fields of the nut 2 (Eq. (17)) and of the tip 2 (Eq. (18)) are given in Table 1. Comparing Eqs. (9) and (17) of Table 1, one can see that they are similar; the main difference is that  $q_s$  and  $q_d$  have opposite signs. This was expected because in the model shown in Fig. 2(a),  $q_d$  and  $q_s$  are in the opposite direction of the longitudinal coordinate axis while in the model shown in the Fig. 2(b) they are in the same direction. The same resemblance can be observed between Eqs. (10) and (18) and between Eqs. (11) and (19).

Once again, we use the condition that at the isothermal section  $x = h$  (which corresponds to  $z = f$ ) the temperatures of the shaft and of the disk are equal. Similarly to Eq. (12), the following equation is written:

$$\begin{aligned} \frac{2}{a^2} \int_0^a \beta(r, e)r dr - q_s \frac{h-e}{k_s} \\ = \frac{2}{(b^2 - a^2)} \int_a^b \xi(r, e)r dr - q_d \frac{1}{h_{c2}} - q_d \frac{h-e}{k_d} \end{aligned} \quad (20)$$

where  $\beta(r, e)$  and  $\xi(r, e)$  are obtained by substituting  $x = e$  into Eqs. (17) and (18), respectively. Solving Eq. (13) for  $q_s$ , substituting it into the equation above and solving it for  $q_d$  one obtains Eq. (21) of Table 1.

The two expressions for the heat flux in the disk  $q_d$ , Eqs. (14) and (21) of Table 1, can be solved simultaneously for  $q_d$  and  $f$ . The expression for the isothermal section is then given by Eq. (23) of Table 1. Using either the left or the right hand side of Eq. (12) one obtains the temperature drop between  $z = 0$  and  $z = f$ . In a similar way, using either the left or the right hand side of Eq. (20), one obtains the temperature drop between  $z = f(x = h)$  and  $z = c + d + e(x = 0)$ . Adding these two temperature drops one obtains the total temperature drop of the heat switch ( $T_2 - T_1$ ) that appears in Eq. (1). Dividing this temperature drop by the heat load  $Q$ , according to Eq. (1), one obtains the expression for the thermal resistance of the heat switch. The final expression for the total thermal resistance of the heat switch, according to the two-dimensional model, is given by:

$$\begin{aligned} R_{2D} = \frac{1}{Q} \left\{ \frac{q_s}{k_s} (c + d + e) + \Psi \left[ \frac{k_{n1} \left( \frac{q_s}{k_s} - \frac{q_d}{k_{n1}} \right)}{\left[ \frac{k_{n1}}{k_s} + \frac{a^2}{(b^2 - a^2)} \right]} \right] \right. \\ \left. + \delta \left[ \frac{k_{n2} \left( \frac{q_s}{k_s} - \frac{q_d}{k_{n2}} \right)}{\left[ \frac{k_{n2}}{k_s} + \frac{a^2}{(b^2 - a^2)} \right]} \right] \right\} \quad (24) \end{aligned}$$

where  $\Psi$  and  $\delta$  are given by Eqs. (15) and (22) of Table 1, respectively.

Table 1

Expressions for temperature fields, heat flux across the disk  $q_d$  and total resistance

$$T(r, z) = T_1 + \frac{q_s}{k_s} z + \frac{8dh_{11}}{\pi^2} \frac{k_{n1}}{k_s} \left( \frac{q_s}{k_s} - \frac{q_d}{k_{n1}} \right) \cdot \sum_{n=0}^{\infty} \frac{(-1)^n}{\Omega_n(2n+1)^2} \left\{ \frac{K_1 \left[ \frac{\pi b}{2d}(2n+1) \right]}{I_1 \left[ \frac{\pi b}{2d}(2n+1) \right]} - \frac{K_1 \left[ \frac{\pi a}{2d}(2n+1) \right]}{I_1 \left[ \frac{\pi a}{2d}(2n+1) \right]} \right\} \cdot I_0 \left[ \frac{\pi r}{2d}(2n+1) \right] \sin \left[ \frac{\pi z}{2d}(2n+1) \right] \quad (9)$$

$$\Theta(r, z) = T_1 + \frac{q_d}{k_{n1}} z + \frac{8dh_{11}}{\pi^2} \left( \frac{q_s}{k_s} - \frac{q_d}{k_{n1}} \right) \sum_{n=0}^{\infty} \frac{(-1)^n}{\Omega_n(2n+1)^2} \cdot \left\{ \frac{K_1 \left[ \frac{\pi b}{2d}(2n+1) \right]}{I_1 \left[ \frac{\pi b}{2d}(2n+1) \right]} I_0 \left[ \frac{\pi r}{2d}(2n+1) \right] + K_0 \left[ \frac{\pi r}{2d}(2n+1) \right] \right\} \sin \left[ \frac{\pi z}{2d}(2n+1) \right] \quad (10)$$

$$\Omega_n = -k_{n1} \frac{\pi}{2d} (2n+1) \left\{ \frac{K_1 \left[ \frac{\pi b}{2d}(2n+1) \right]}{I_1 \left[ \frac{\pi b}{2d}(2n+1) \right]} I_1 \left[ \frac{\pi a}{2d}(2n+1) \right] - K_1 \left[ \frac{\pi a}{2d}(2n+1) \right] \right\} + h_{11} \left\{ \frac{k_{n1}}{k_s} \frac{K_1 \left[ \frac{\pi a}{2d}(2n+1) \right]}{I_1 \left[ \frac{\pi a}{2d}(2n+1) \right]} I_0 \left[ \frac{\pi a}{2d}(2n+1) \right] + K_0 \left[ \frac{\pi a}{2d}(2n+1) \right] \right\} \quad (11)$$

$$q_d = \frac{Q}{\pi a^2} \cdot \frac{f + \Psi}{k_s \left\{ \frac{f-d}{k_d} + \frac{d}{k_{n1}} + \frac{1}{h_{c1}} + \left( \frac{b^2-a^2}{a^2} \right) \frac{f}{k_s} + \Psi \left[ \frac{b^2-a^2}{a^2 k_s} + \frac{1}{k_{n1}} \right] \right\}} \quad (14)$$

$$\Psi = \frac{32d^2 h_{11}}{\pi^3} \left[ \frac{k_{n1}}{a k_s} + \frac{a}{(b^2-a^2)} \right] \sum_{n=0}^{\infty} \frac{1}{\Omega_n(2n+1)^3} \left\{ \frac{K_1 \left[ \frac{\pi b}{2d}(2n+1) \right]}{I_1 \left[ \frac{\pi b}{2d}(2n+1) \right]} I_1 \left[ \frac{\pi a}{2d}(2n+1) \right] - K_1 \left[ \frac{\pi a}{2d}(2n+1) \right] \right\} \quad (15)$$

$$\beta(r, x) = T_2 - \frac{q_s}{k_s} x - \frac{8eh_{12}}{\pi^2} \frac{k_{n2}}{k_s} \left( \frac{q_s}{k_s} - \frac{q_d}{k_{n2}} \right) \sum_{n=0}^{\infty} \frac{(-1)^n}{\Gamma_n(2n+1)^2} \cdot \left\{ \frac{K_1 \left[ \frac{\pi b}{2e}(2n+1) \right]}{I_1 \left[ \frac{\pi b}{2e}(2n+1) \right]} - \frac{K_1 \left[ \frac{\pi a}{2e}(2n+1) \right]}{I_1 \left[ \frac{\pi a}{2e}(2n+1) \right]} \right\} I_0 \left[ \frac{\pi r}{2e}(2n+1) \right] \sin \left[ \frac{\pi x}{2e}(2n+1) \right] \quad (17)$$

$$\zeta(r, x) = T_2 - \frac{q_d}{k_{n2}} x - \frac{8eh_{12}}{\pi^2} \left( \frac{q_s}{k_s} - \frac{q_d}{k_{n2}} \right) \sum_{n=0}^{\infty} \frac{(-1)^n}{\Gamma_n(2n+1)^2} \cdot \left\{ \frac{K_1 \left[ \frac{\pi b}{2e}(2n+1) \right]}{I_1 \left[ \frac{\pi b}{2e}(2n+1) \right]} I_0 \left[ \frac{\pi r}{2e}(2n+1) \right] + K_0 \left[ \frac{\pi r}{2e}(2n+1) \right] \right\} \sin \left[ \frac{\pi x}{2e}(2n+1) \right] \quad (18)$$

$$\Gamma_n = -k_{n2} \frac{\pi}{2e} (2n+1) \left\{ \frac{K_1 \left[ \frac{\pi b}{2e}(2n+1) \right]}{I_1 \left[ \frac{\pi b}{2e}(2n+1) \right]} I_1 \left[ \frac{\pi a}{2e}(2n+1) \right] - K_1 \left[ \frac{\pi a}{2e}(2n+1) \right] \right\} + h_{12} \left\{ \frac{k_{n2}}{k_s} \frac{K_1 \left[ \frac{\pi a}{2e}(2n+1) \right]}{I_1 \left[ \frac{\pi a}{2e}(2n+1) \right]} I_0 \left[ \frac{\pi a}{2e}(2n+1) \right] + K_0 \left[ \frac{\pi a}{2e}(2n+1) \right] \right\} \quad (19)$$

$$q_d = \frac{Q}{\pi a^2} \frac{h + \delta}{k_s \left\{ \frac{h-e}{k_d} + \frac{e}{k_{n2}} + \frac{1}{h_{c2}} + \left( \frac{b^2-a^2}{a^2} \right) \frac{h}{k_s} + \delta \left[ \frac{b^2-a^2}{a^2 k_s} + \frac{1}{k_{n2}} \right] \right\}} \quad (21)$$

$$\delta = \frac{32e^2 h_{12}}{\pi^3} \left[ \frac{k_{n2}}{a k_s} + \frac{a}{(b^2-a^2)} \right] \cdot \sum_{n=0}^{\infty} \frac{1}{\Gamma_n(2n+1)^3} \left\{ \frac{K_1 \left[ \frac{\pi b}{2e}(2n+1) \right]}{I_1 \left[ \frac{\pi b}{2e}(2n+1) \right]} I_1 \left[ \frac{\pi a}{2e}(2n+1) \right] - K_1 \left[ \frac{\pi a}{2e}(2n+1) \right] \right\} \quad (22)$$

$$f = d + \frac{(e+c+\delta) \left( \frac{d+\Psi}{k_{n1}} + \frac{1}{h_{c1}} \right) - (d+\Psi) \left( \frac{\delta+e}{k_{n2}} + \frac{e}{k_d} + \frac{1}{h_{c2}} \right)}{(\delta+e) \left( \frac{1}{k_{n2}} - \frac{1}{k_d} \right) + \left( \frac{1}{k_{n1}} - \frac{1}{k_d} \right) (d+\Psi) + \frac{1}{h_{c1}} + \frac{1}{h_{c2}}} \quad (23)$$

### 2.2. One-dimensional heat conduction model

In the development of one-dimensional model, heat is assumed to flow only in the axial direction of the heat switch. The thermal contact resistances of the threads are considered to be infinities. The total thermal resistance of the heat switch is computed as the total resistance of the analog electric circuit shown in Fig. 2(d). In this analog circuit, the  $R_{m,i}$  are material resistances. The subscript “ $i$ ” can be s (shaft), d (disk), n1 (nut 1) and n2 (nut 2). The resistances  $R_{c,n1-d}$  and  $R_{c,n2-d}$  are the contact resistances between the nut 1 and the disk and between the nut 2 and the disk, respectively. These resistances are given by the following expressions:

$$R_{m,n1} = \frac{d}{k_{n1}\pi(b^2 - a^2)} \tag{25}$$

$$R_{m,n2} = \frac{e}{k_{n2}\pi(b^2 - a^2)} \tag{26}$$

$$R_{m,d} = \frac{c}{k_d\pi(b^2 - a^2)} \tag{27}$$

$$R_{m,s} = \frac{c + d + e}{k_s\pi a^2} \tag{28}$$

$$R_{c,n1-d} = \frac{1}{h_{c1}\pi(b^2 - a^2)} \tag{29}$$

$$R_{c,n2-d} = \frac{1}{h_{c2}\pi(b^2 - a^2)} \tag{30}$$

Combining these resistances according to the equivalent electric circuit, the overall thermal resistance of the heat switch, assuming one-dimensional heat flow, is given by:

$$R_{1D} = \frac{1}{\pi} \left[ \frac{k_s a^2}{c + d + e} + \frac{(b^2 - a^2)}{\frac{d}{k_{n1}} + \frac{1}{h_{c1}} + \frac{c}{k_d} + \frac{1}{h_{c2}} + \frac{e}{k_{n2}}} \right]^{-1} \tag{31}$$

### 2.3. Thermal contact conductance models

Several studies on the contact conductance between conforming rough surfaces are available in the literature [7–10]. The model proposed by Mikic [9] for elastic deformation of asperities, which is based on the plastic model of Cooper et al. [8], is used in this work. The reason for choosing this particular model will be discussed later. The elastic model of Mikic [9] can be represented by the following correlation:

$$\frac{h_c}{k_h} \frac{\sigma}{m} = 1.55 \left( \frac{P\sqrt{2}}{E'm} \right)^{0.94} \tag{32}$$

where

$$E' = \left( \frac{1 - \nu_A^2}{E_A} + \frac{1 - \nu_B^2}{E_B} \right)^{-1} \tag{33}$$

is the Effective Young Modulus and  $k_h = 2k_A k_B / (k_A + k_B)$  is the harmonic mean of the thermal conductivities of the contacting bodies. The Poisson’s ratio is  $\nu$ ,  $P$  is the apparent contact pressure, and  $\sigma$  and  $m$  are the combined RMS roughness and mean absolute slope of the contacting surfaces, respectively.

It is assumed that the contact conductances are uniform in the contacting interfaces between the disk and the nuts. A uniform contact conductance distribution can be obtained when flat surfaces are pressed against each other under uniform contact pressure. Although nearly flat surfaces can be obtained in practical applications, similar studies [12–14] showed that the actual contact pressure presents non-uniform distribution at the interfaces between the disk and the nuts. Near the shaft, the contact pressure distribution presents a maximum value, and decreases as the radius increases. However, the more rigid the nuts, the more uniform is the contact pressure distribution. In this work, it is assumed that the nuts are infinitely rigid and that the contacting surfaces are nominally flat. This condition can be achieved by designing the nuts as thick as possible. Considering the nuts infinitely rigid, the disk experiences nearly one-dimensional compression stress, and the contact pressure at a given temperature ( $T_m$ ) is computed with the following expression:

$$P = P_0 + \frac{(\bar{\alpha}_d - \bar{\alpha}_s)}{\left[ \frac{1}{E_s} \frac{(b^2 - a^2)}{a^2} + \frac{1}{E_d} \right]} (T_m - T_0) \tag{34}$$

where  $\bar{\alpha}$  is the mean value of the thermal expansion coefficient between  $T_0$ , the temperature at which the heat switch is assembled, and  $T_m$ . The contact pressure at  $T_0$  is  $P_0$ . Mantelli and Yovanovich [15] and Katwijk and Bennet [16] presented expressions similar to Eq. (34) in order to predict the mean contact pressure of bolted joints as a function of the mean temperature of the joint.

There are no studies in the literature about the contact conductance of threaded contacts. The existing experimental and theoretical contact conductance studies are based on the contact between nominally flat (like Mikic’s [9] model above) and/or ellipsoid surfaces. Since it is difficult to predict the thermal contact conductance of threads, the influence of the thread conductances on the total resistance of the heat switch will be parametrically analyzed in the next section. As it will be seen, the thermal contact conductance of the threads can be neglected without significant losses.

### 3. Study of the influence of the thread contact conductance on the heat switch total thermal resistance

In this section, the effect of the thread contact conductance on the heat switch total thermal resistance is analyzed. The analysis is conducted in the

non-dimensional form. The following dimensionless parameters are employed:

$$\left\{ \begin{aligned} b^* &= \frac{b}{a}, c^* = \frac{c}{a}, d^* = \frac{d}{a}, e^* = \frac{e}{a}, k_i^* = \frac{k_i}{k_s}, h_c^* = \frac{h_c a}{k_s} \\ R^* &= \frac{R \pi k_s a^2}{c + d + e}, P_O^* = \frac{P_0}{E'}, E^* = \frac{E}{E'}, \sigma^* = \frac{\sigma}{1.07 a m^{0.06}} \end{aligned} \right\} \quad (35)$$

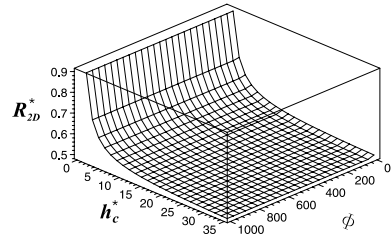
In order to simplify this analysis, it is assumed that the contact conductances at both sides of the disk are equal, that is,  $h_{c1}^* = h_{c2}^* = h_c^*$ . A dimensionless parameter  $\Phi$  is defined as the ratio between the thread contact conductance and the disk–nut contact conductance:

$$\Phi = \frac{h_{t1}^*}{h_{c1}^*} = \frac{h_{t2}^*}{h_{c2}^*} \quad (36)$$

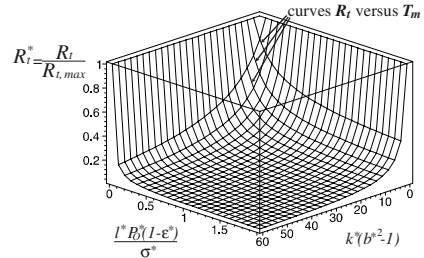
Fig. 3(a) shows the total thermal resistance of the heat switch computed using the analytical two-dimensional model ( $R_{2D}^*$ ) as a function of the contact conductance ( $h_c^* = h_{c1}^* = h_{c2}^*$ ) and for  $\Phi$  ranging from 0 to 1000. In this graph, constant values of  $k_{n1}^* = k_{n2}^* = k_d^* = 0.5$  were assumed, which correspond to the conductivities of the materials (SS 304 and Ti-alloy) used in heat switch prototype employed in the experimental study presented later. The lower limit of  $\Phi$  corresponds to the case where the contact conductance of the threads are zero, and the upper limit corresponds to the case where the conductances of the threads are 1000 times larger than the conductances of the disk–nut interfaces. As it can be seen in this graph, the thermal resistance increases as  $h_c^*$  decreases, regardless of the value of  $\Phi$ . For  $\Phi = 0$ , the thermal resistances are only slightly larger than for  $\Phi = 1000$ . In other words,  $\Phi$  has little influence on the thermal resistance of the heat switch. Therefore, the error associated with a poor prediction of the thread conductance is very small. This is very convenient given the difficulty in predicting the thread conductance.

From this discussion, it is observed that the thermal resistance of the thread can be considered infinity, that is,  $\Phi = 0$ . By doing this, the heat flux through the thread is being ignored and the heat flow inside the heat switch is one-dimensional, along the axial direction. For  $\Phi = 0$ , the heat switch total resistance value computed using the two-dimensional model is exactly the same as the value computed using the one-dimensional model, that is,  $R_{2D}(\Phi = 0) = R_{1D}$ . Therefore, the one-dimensional model is sufficiently accurate to predict the total resistance of the switch, which is good, given the complex form of the equations that constitute the two-dimensional model (Eqs. (11), (15), (19), (22), (24)) in comparison with the one-dimensional model (Eq. (31)).

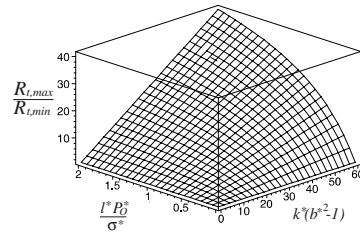
In order to close this discussion about the difference between the values of total thermal resistance computed using the two models presented previously, it is convenient to perform an analysis in terms of the Biot number



(a)



(b)



(c)

Fig. 3. Non-dimensional parametric analysis. (a)  $R_{2D}^*$  as a function of  $h_c^*$  and  $\Phi$ . (b) Dimensionless total thermal resistance of the heat switch  $R_t^*$ . (c) Switching ratio of the heat switch  $R_{t,max}/R_{t,min}$ .

( $Bi = hL/k$ ) in the radial direction inside the nuts. According to Table 2, which gives the geometrical parameters and physical properties of the heat switch employed in the experimental study (presented later on), a typical heat switch nut made of stainless steel has a conductivity of  $k = 12$  W/mK and has a characteristic length of  $L = b - a = 0.013$  m. A typical range of contact conductance values  $h_c$  for stainless steel is between 0 (for 0 contact pressure) and 2000 W/m<sup>2</sup> K (for contact pressure of approximately 2 MPa). Therefore, the Biot number ranges from 0 to approximately 2.1 for this example. For most of the operational range of the heat switch, the Biot number is larger than 0.1, and therefore the one-dimensional temperature field assumption in the nuts could lead to significant errors. However, the aim is to predict the total thermal resistance of the heat switch and not the temperature field. For total thermal resistance computation purposes, the one-dimensional model is accurate, despite the Biot number in the radial direction of the nut being larger than 0.1.

Table 2  
Geometrical parameters and physical properties of the heat switch tested

Parameter	Value	Parameter	Value
$a$ [m]	0.003	$E_d$ [GPa]	200
$b$ [m]	0.016	$E_s$ [Gpa]	115
$c$ [m]	0.016	$v_{n1} = v_{n2} = v_d$	0.3
$d$ [m]	0.020	$\sigma$ [ $\mu\text{m}$ ]	2.2
$e$ [m]	0.016	$m$ [ ]	0.1
$k_{n1} = k_{n2} = k_d$ [W/mK]	11 <sup>a</sup>	$k_s$ [W/mK]	30 <sup>a</sup>
	15 <sup>b</sup>		30 <sup>b</sup>

<sup>a</sup> At 100 K.

<sup>b</sup> At 300 K.

### 3.1. Non-dimensional parametric analysis

In this section, a parametric analysis is conducted in order to study the relative influence of the design parameters (dimensions and materials) on the total thermal resistance of the heat switch. The analyses will be conducted in a non-dimensional form. The one-dimensional conduction model, which was shown in the previous section to be accurate, is used here.

In order to simplify the analyses that follows, it will be assumed that the two nuts have the same thickness ( $d = e$ ) and that they are made of the same material. It will be further assumed that the materials of the nuts are the same as the material of the disk, and that their physical properties are equal. With these assumptions, and by substituting the non-dimensional parameters (Eq. (35)) in the expressions that constitute the theoretical model for the total resistance of the heat switch (Eqs. (31)–(34)), after some algebraic manipulations, one obtains:

$$R_t^* = R_{tD}^* = \left[ 1 + \frac{k^*(b^{*2} - 1)}{1 + \frac{\sigma^*}{l^*P_0^*(1-\varepsilon^*)}} \right]^{-1} \quad (37)$$

where:

$$\varepsilon^* = \frac{\Delta T(\bar{\alpha}_d - \bar{\alpha}_s)}{P_0^* \left[ \frac{(b^{*2}-1)}{E_s^*} + \frac{1}{E_d^*} \right]} \quad (38)$$

The parameter  $l^*$ , appearing in Eq. (37), is the dimensionless total length of the heat switch ( $l^* = c^* + d^* + e^*$ ). In Eq. (38),  $\Delta T = T_0 - T_m$  is the temperature decrease experienced by the heat switch between the assembly temperature  $T_0$  and a given temperature  $T_m$ . The parameter  $\varepsilon^*$ , which appears in Eq. (37) and is defined according to Eq. (38), is named the dimensionless differential thermal expansion parameter. It can be interpreted as the ratio between the amount of differential thermal expansion at a given  $\Delta T$  and the amount of thermal expansion necessary for the complete decoupling of the heat switch. Therefore, during the operation of the heat switch,  $\varepsilon^*$  assume values between 0 (assembly) and 1 (decoupling).

According to the definition of the dimensionless parameters given by Eq. (35), the dimensionless total thermal resistance  $R_t^*$  (Eq. (37)) represents the ratio between the resistance at a given temperature  $T_m$  and the maximum possible resistance (when the heat switch is decoupled). Therefore,  $R_t^*$  is 1 at the decoupling temperature. When the disk is coupled,  $0 < R_t^* < 1$ . Note that  $R_t^*$  can not reach zero because the material and contact resistances are always larger than zero.

Fig. 3(b) shows a graph of the dimensionless total resistance of the heat switch  $R_t^*$  as a function of the two dimensionless groups  $[k^*(b^{*2} - 1)]$  and  $[l^*P_0^*(1 - \varepsilon^*)/\sigma^*]$ , that appear in Eq. (37). The dimensionless group  $[k^*(b^{*2} - 1)]$  represents the ratio between the disk–nuts path conductance and the shaft path conductance. The larger are  $k^*$  (conductivity) and  $b^{*2}$  (cross-sectional area) of the disk and the nuts, the smaller is the total resistance of the heat switch. The dimensionless group  $[l^*P_0^*(1 - \varepsilon^*)/\sigma^*]$  represents the ratio between the disk/nuts contact conductances and the shaft conductance. If the contact conductances are large (small roughness  $\sigma^*$ , small thermal expansion  $\varepsilon^*$ , and large assembly pressure  $P_0^*$ ) in comparison with the material thermal conductance of the shaft ( $1/l^*$ ), the total resistance of the heat switch is small. It can be also seen that if one of these two non-dimensional groups is zero, the total resistance of the heat switch reaches its maximum value ( $R_t^* = 1$ ). The dimensionless group  $[l^*P_0^*(1 - \varepsilon^*)/\sigma^*]$  is zero when  $\varepsilon^* = 1$ , that is, when the heat switch is decoupled. On the other hand, the dimensionless group  $[k^*(b^{*2} - 1)]$  can not be equal to zero in practical applications because both  $b^* = b/a > 1$  and  $k^* > 0$ .

The dimensionless group  $[l^*P_0^*(1 - \varepsilon^*)/\sigma^*]$  varies during the operation of the heat switch because  $\varepsilon^*$  is proportional to  $\Delta T$  (Eq. (38)). Therefore, as the dimensionless group  $[l^*P_0^*(1 - \varepsilon^*)/\sigma^*]$  is directly proportional to  $\Delta T$ , the curves of constant  $[k^*(b^{*2} - 1)]$  of Fig. 3(b) represent the possible curves of thermal resistance versus mean temperature of the heat switch. As it can be seen, when  $[l^*P_0^*(1 - \varepsilon^*)/\sigma^*] > 0.5$  and  $[k^*(b^{*2} - 1)] > 20$ , the values of total resistance  $R_t^*$  are small and are almost constant with temperature. On the other hand, the total resistance of the heat switch changes very

quickly with temperature when  $[I^*P_0^*(1 - \varepsilon^*)/\sigma^*] < 0.1$ . The smaller the value of  $[k^*(b^{*2} - 1)]$ , the smoother the transition between the minimum and the maximum total resistances. Therefore, the behavior of the total resistance of the heat switch with temperature can be determined during the design process by choosing appropriate values for these two non-dimensional groups.

Another important design parameter is the switching ratio of the heat switch, defined as the ratio between the maximum and the minimum possible thermal resistances. Substituting  $\varepsilon^* = 0$  in Eq. (37), one obtains the minimum dimensionless total resistance of the heat switch. The minimum dimensionless resistance represents also the ratio between the minimum and the maximum total resistances. Therefore, for  $\varepsilon^* = 0$  the parameter  $1/R_t^*$  represents the switching ratio of the heat switch, that is,  $1/R_t^* = R_{t,\max}/R_{t,\min}$ . Fig. 3(c) shows a graph of the switching ratio as a function of the dimensionless groups  $[k^*(b^{*2} - 1)]$  and  $[I^*P_0^*/\sigma^*]$ . As it can be seen in this graph, the switching ratio increases with both  $[k^*(b^{*2} - 1)]$  and  $[I^*P_0^*/\sigma^*]$ .

Substituting  $\varepsilon^* = 1$  in Eq. (38) and rearranging the resulting expression one obtains:

$$[\Delta T(\bar{\alpha}_d - \bar{\alpha}_s)]_{\max} = P_0^* \left[ \frac{(b^{*2} - 1)}{E_s^*} + \frac{1}{E_d^*} \right] \quad (39)$$

which is the maximum amount of differential thermal expansion that the heat switch needs to decouple. As it can be seen from this equation, the decoupling temperature  $[\Delta T]_{\max}$  depends on the thermal expansion coefficients and on the elastic properties of the materials, as well as the ratio between the heat switch external radius and the shaft radius ( $b^*$ ). Given the decoupling temperature, the equation above can be employed during the design process in order to select the materials and the ratio  $b^* = b/a$  of the heat switch.

When the heat switch is decoupled, conduction through the shaft is the only possible heat path across the heat switch. As the heat transfer is one-dimensional along the shaft, the maximum resistance of the heat switch is defined by the geometry and the thermal conductivity of the shaft. Therefore, in order to obtain a high thermal resistance, the shaft must be made of a material possessing low thermal conductivity and must have a high length-to-area ratio.

#### 4. Experimental study

The experimental study consists of measuring the total thermal resistance as a function of temperature (between 100 and 300 K) of a prototype of the heat switch. The study was conducted in a vacuum thermal test facility at the Satellite Thermal Control Laboratory of the Federal University of Santa Catarina.

##### 4.1. Experimental set-up

The experimental set-up employed in this study is shown in Fig. 4(a). It consists basically of a vacuum chamber, a cold plate, a thin circular electric heater and a radiation shield. The vacuum inside the chamber is  $4 \times 10^{-6}$  mbar. The cold plate consists of a hollow copper cylinder, filled with liquid Nitrogen. The heat switch is placed between the cold plate and the electric heater. MLI blankets cover the electric heater in order to avoid thermal radiation losses to the radiation shield. The radiation shield consists of an aluminum cup placed over the cold plate and surrounding the heat switch. During the tests, the radiation shield reaches the cold plate temperature, and absorbs all radiation coming from the external environment. 15 T type, gage #40 thermocouples, located as shown in Fig. 4(b), measured the temperatures in several points of the heat switch.

The prototype of the heat switch was made of Stainless Steel 304 (nuts and disk) and titanium alloy 98.9%Ti–1.1%Al (shaft). Table 2 shows the numerical values of the geometrical parameters and physical properties of the prototype tested. The values of thermal

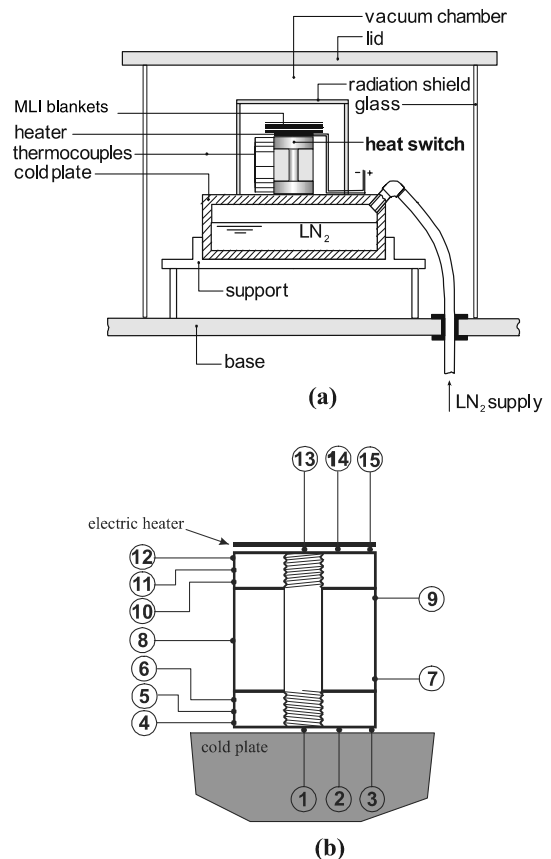


Fig. 4. Experimental set-up (a) and thermocouple locations (b).

expansion coefficients are not presented in this table because no reliable source was found in the literature for this property. However, the difference between the thermal expansion coefficients  $\bar{\alpha}_d - \bar{\alpha}_s$ , which is required as an input to the models, was measured in the experimental study that is presented later. The contacting surfaces of the nuts and disk were lapped in order to avoid flatness deviations. The flatness deviations of the surfaces were measured and were found to be less than 1  $\mu\text{m}$ . The contacting surfaces were then bead blasted in order to get isotropic rough surfaces with approximately Gaussian roughness height distributions.

As the elastic properties  $E$  and  $\nu$  of SS304 and Ti-Alloy do not show significant variation with temperature between 100 and 300 K [17], they are assumed to be constant during the tests. The thermal conductivities of the stainless steel and of the Ti-alloy were measured from cylindrical specimens machined from the same stock bars as the heat switch. The conductivities were measured at two mean temperatures levels (100 and 300 K), and employing the same experimental set-up described before. For the conductivity measurements, cylindrical specimens were placed between two cylindrical fluxmeters made of ARMCO Iron. The three cylinders were then placed over the cold plate, with the electric heater on the top. As the thermal conductivity of the ARMCO is well known, the heat flux crossing the test column can be estimated very accurately. The measured values of the thermal conductivities of SS 304 were 11 and 15  $\text{W/m}^2 \text{K}$  at 100 and 300 K, respectively. These values are in close agreement with the values of 10 and 15.5  $\text{W/m}^2 \text{K}$ , respectively, found by other researchers [17]. This result shows that the experimental set-up gives accurate results. The thermal conductivities at temperatures between 100 and 300 K are estimated by linear interpolation. The measured value of the thermal conductivity of the Ti-alloy was 30  $\text{W/m}^2 \text{K}$  at both 100 and 300 K.

#### 4.2. Test procedure

The total thermal resistance of the heat switch was obtained through the measurement of the temperatures along the heat switch for several power levels of the electric heater. The temperatures were taken at steady-state conditions, which were achieved approximately 1 h after the power level was set. The total thermal resistance was calculated as:

$$R_t = \frac{T_{m1} - T_{m2}}{Q} \quad (40)$$

where

$$T_{m1} = \frac{T_{13} + T_{14} + T_{15}}{3} \quad (41)$$

$$T_{m2} = \frac{T_1 + T_2 + T_3}{3} \quad (42)$$

are the average temperatures at the top and the bottom surfaces of the heat switch, respectively (see Fig. 4(b)). The total heat flux  $Q$  [W] crossing the heat switch, is given by:

$$Q = 0.9VI \quad (43)$$

where  $V$  [V] is the voltage and  $I$  [A] is the current intensity of the DC power supply. The correction factor 0.9 was introduced into the expression above in order to take into account for the heat loss from the heater to the cold plate by conduction through the power supply wires. This means that 10% of the heat dissipated in the heater is conducted to the cold plate through the power supply wires without crossing the heat switch. This value was obtained during the thermal conductivity measurement tests by dividing the total heat flux crossing the heat fluxmeters by the electrical power supplied to the heater ( $VI$ ). The value of 0.9 is the average of 14 readings at different power levels of the electric heater. The standard deviation of these 14 readings was 0.05.

The mean temperature of the heat switch is defined as:

$$T_m = \frac{T_{m1} + T_{m2}}{2} \quad (44)$$

A correlation between the contact pressure  $P_0$  at room temperature  $T_0$  and the mounting torque  $M_T$  was previously established by means of a load cell and a torque meter. It is given by:

$$P_0 = 853,700M_T \quad (45)$$

Therefore, given the mounting torque  $M_T$  it is possible to evaluate the contact pressure at room temperature ( $P_0$ ), which is used in Eq. (34). The pressure distribution over the contacting surfaces was also measured. A Fuji-film<sup>®</sup> pressure sensitive film was used for this purpose. The film was placed between the contacting surfaces and when the pressure was applied, the color density of the film changed according to the pressure level. The contact pressure variations along the contact interfaces of the heat switch were found to be less than 10%.

#### 4.3. Uncertainty analysis

The thermocouples were calibrated at room temperature and at the temperature of saturated liquid nitrogen. The uncertainties of the temperature readings were  $\pm 0.3 \text{ K}$ . The uncertainties of the voltage and the current intensity were  $\pm 0.01 \text{ V}$  and  $\pm 0.01 \text{ A}$ , respectively. The total percentual uncertainty of the heat flux crossing the heat switch ( $Q$ ) is  $\pm 4\%$ . Following the methodology of error propagation described in Holman [18], the maximum uncertainty of the measurements of the heat switch total thermal resistance, computed using Eqs. (40)–(43),

is  $\pm 4\%$ . The uncertainty in the computation of the mean temperature of the heat switch (Eq. (44)) is  $\pm 0.2$  K.

### 5. Experimental results and comparison with theory

The heat switch was assembled with a torque of  $M_T = 2.4$  N m, which corresponds to an initial contact pressure of  $P_0 = 2$  MPa (Eq. (45)) at a temperature level of  $T_0 = 300$  K. The tests were performed in descending power levels of the electric heater. The following procedure was applied: starting from equilibrium at room temperature, the cold plate was filled with  $LN_2$  and the heater was turned “on”. After the thermal equilibrium was achieved, the temperature readings were taken and then another electric heater power level was set. This procedure was repeated for eight power levels.

The measured temperature distributions of the heat switch for eight power levels are shown in Fig. 5(a). The numbers appearing in the abscissa of this graph correspond to the thermocouple numbers shown in Fig. 4(b). For each one of the curves shown in Fig. 5, one can observe three well defined regions: nut 1 (thermocouples 1–6), the disk (thermocouples 7–9) and the nut 2, (thermocouples 10–15). Between thermocouples 6 and 7, all the curves present discontinuities, which are due to the contact resistance between the nut and the disk. The same is observed between thermocouples 9 and 10.

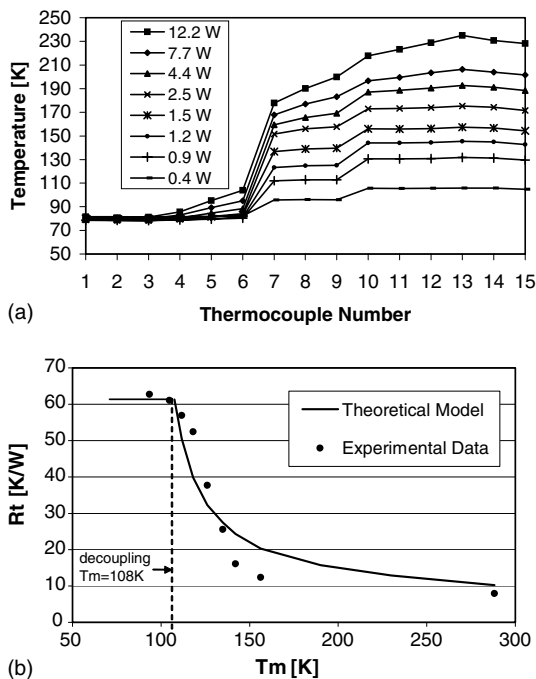


Fig. 5. Experimental results: temperature readings (a) and comparison between data and theory (b).

Fig. 5(b) shows the measured values of the total thermal resistance ( $R_t$ ) as a function of the mean temperature level of the heat switch ( $T_m$ ). One can see nine data points in this graphic, which correspond to the eight power levels shown in Fig. 5(a), plus another point collected previously at room temperature ( $T_m = 288$  K). The data point at room temperature was collected using water as the coolant of the cold plate instead of  $LN_2$ , which was used for the other eight points. The vertical dashed line shown in the graphic of Fig. 5(b) corresponds to the decoupling temperature. The decoupling temperature is detected during the tests by inspecting the time spent by the disk to reach steady-state. When the heat switch is coupled, the disk temperature readings reach steady-state at the same time as the rest of the heat switch. When the heat switch is decoupled, the disk temperature readings keep decreasing even after the rest of the heat switch had achieved steady-state. For 1.2 W ( $T_m = 111.4$  K) the heat switch was still coupled and for 0.9 W ( $T_m = 104.7$  K) the heat switch was already decoupled. Therefore, it can be concluded that the decoupling occurred between 111.3 and 104.7 K. In this work, an average of this two values is adopted as the decoupling temperature, that is  $T_{\text{decoupling}} = 108 \pm 3.3$  K.

Knowing the decoupling temperature, the mean difference between the thermal expansion coefficients was computed using Eq. (34) and presented a value of  $\bar{\alpha}_d - \bar{\alpha}_s = 2.4 \times 10^{-6}$  K $^{-1}$ . Substituting this value and the other required input parameters (Table 2) into the theoretical models for prediction of the total thermal resistance of the heat switch (Eqs. (31)–(34)), one obtains the curve shown in Fig. 5(b). As it can be seen in this graphic, the comparison between theory and experiment is fairly good. For  $130 < T_m < 300$  K, the theory overpredicts the experimental data with a maximum difference of 64%. On the other hand, for  $T_m < 130$  K the models underpredict the experimental data with a maximum difference of 25%. The minimum difference between theory and experiment is only 0.3% at  $T_m = 104$  K. It is convenient to recall that the value of  $\bar{\alpha}_d - \bar{\alpha}_s$  obtained here is a mean over the temperature range between  $T_0$  and  $T_m$ . However, Ref. [17] shows that the thermal expansion coefficients for SS 304 and Ti-alloys present more or less the same trend of variation with temperature. In other words, despite the fact that the absolute values for both SS 304 and Ti-alloys vary with temperature, the difference between them is practically constant. Therefore, assuming a constant value of  $\bar{\alpha}_d - \bar{\alpha}_s$  for temperature ranges other than between  $T_0$  and  $T_m$  should not lead to considerable errors.

If a plastic model for contact conductance, such as the model of Yovanovich [10], is employed instead of the elastic model of Mikic [9], slightly higher contact conductances would be predicted, and the theoretical curve of Fig. 5(b) would lie slightly lower. The difference between these two models can be neglected in this case.

Sridhar and Yovanovich [19] made an extensive review of the existing contact conductance models available in the literature. They found that the plastic model of Yovanovich [10] and the elastic model of Mikic [9] were in good agreement with several other models investigated and also with experimental data. According to Sridhar and Yovanovich [19], these two models are also simpler and easier to manipulate than the other models. Despite the two contact conductance models tested here predicted similar values and they were shown by other researchers to be very accurate to predict experimental data other from other researchers, it is believed that they are not appropriate for this particular study. It is believed that the differences between the theoretical predictions and the experimental data are due to the inaccuracy of the thermal contact conductance model. It is known from other studies, such as Milanez et al. [11], McWaid [20] and Li et al. [21], among others, that during the unloading of the contact pressure, thermal contact conductance of stainless steel is larger than during loading. This phenomenon is known as the hysteresis effect of thermal contact conductance. The hysteresis effect is a consequence of plastic deformations of the contacting asperities occurred during the assembly of the heat switch. The asperities do not recover their original shape during the unloading of the contact pressure, and therefore, the real contact area during unloading is larger than during loading. It is also reported by Sridhar and Yovanovich [10], that at light contact pressures, thermal contact conductance present an unusual behavior and are not accurately predicted by the models available. Milanez et al. [11] proposed an explanation for this behavior: the highest contacting asperities are shorter than predicted by the models, therefore the mean separation gap at light contact pressures is smaller than predicted by the theory, and as a consequence the thermal contact conductance is larger than predicted. The hysteresis effect and the light contact pressure effect are very difficult to predict and further studies are needed in this regard.

## 6. Summary and conclusions

This work presents theoretical and experimental studies of a bimetallic heat switch for space applications. The heat switch is passively actuated and presents a thermal resistance which is a function of the mean temperature. Two analytical models were developed to predict the thermal resistance of the heat switch: a two-dimensional model and an one-dimensional model.

An analysis of the influence of the thermal contact conductance of the threads on the heat switch total resistance is conducted using the two-dimensional model. The analysis showed that the total thermal resistance of the heat switch is little affected by the value of the

contact conductance of the threads. The analysis also shows that the temperature field of the heat switch is basically one-dimensional along the axial direction and that the one-dimensional model is accurate to predict the total thermal resistance of the heat switch. A non-dimensional parametric analysis is also conducted in order to study the influence of the parameters that affect the total thermal resistance of the heat switch. The non-dimensional analysis showed that two dimensionless groups govern the behavior of the total thermal resistance of the heat switch.

The theoretical models are compared against experimental data collected from a prototype of the heat switch. The comparison shows a fairly good agreement between the theoretical prediction and the experimental data. It is believed that the differences observed between the predicted and the measured values of the total thermal resistance of the prototype is due to the inaccurate prediction of the thermal contact conductance of the disk–nut interfaces. The hysteresis effect of thermal contact conductance and the relatively light contact pressures seem to play an important role on the total resistance of the heat switch, but it is not being accounted for because they are difficult to predict. Further studies are needed in the thermal contact conductance field, especially for contacts under the operational conditions of the heat switch.

## Acknowledgements

The authors would like to acknowledge the Brazilian Space Agency—AEB, and National Council of Research and Development—CNPq, for supporting this project.

## References

- [1] D.J. Frank, T.C. Nast, Getter-activated cryogenic thermal switch, in: *Proceedings of Cryogenic Engineering Conference*, Cambridge, 1982, pp. 933–940.
- [2] T. Nast, G. Bell, C. Barnes, Development of gas gap cryogenic thermal switch, in: *Advances in Cryogenic Engineering*, vol. 27, Plenum Press, New York, 1982, pp. 1117–1124.
- [3] L. Naes, T. Nast, A self actuated thermal switch for operation with redundant mechanical refrigerators, in: *Proceedings of Cryogenic Engineering Conference*, Cambridge, 1985, pp. 925–932.
- [4] S. Van Oost, G. Bekaert, R.S. Bhatti, S. Scull, C. Jewell, A heat switch for space cryocooler applications, in: *Proceedings of the Fourth European Symposium on Space Environmental and Control Systems*, 1991, pp. 209–216.
- [5] F.H. Milanez, M.B.H. Mantelli, A new passive heat switch conception for space applications, ASME Paper No. NHTC99-0267, in: *Proceedings of the 33rd National Heat*

- Transfer Conference, 15–17 August, Albuquerque, NM, 1999.
- [6] V.S. Arpaci, *Conduction Heat Transfer*, Addison-Wesley Publishing Company, Reading, MA, 1966.
- [7] J. Greenwood, J. Williamson, Contact of nominally flat surfaces, *Proc. R. Soc. London A* 295 (1966) 300–319.
- [8] M. Cooper, B. Mikic, M. Yovanovich, Thermal contact conductance, *Int. J. Heat Mass Transfer* 12 (1969) 279–300.
- [9] B.B. Mikic, Thermal contact conductance; theoretical considerations, *Int. J. Heat Mass Transfer* 17 (1974) 205–214.
- [10] M.M. Yovanovich, Thermal contact correlations, spacecraft radiative heat transfer and temperature control, in: T.E. Horton (Ed.), *Progress in Astronautics and Aeronautics*, vol. 83, NY, 1981, pp. 83–95.
- [11] F.H. Milanez, J.R. Culham, M.M. Yovanovich, Experimental study on the hysteresis effect of thermal contact conductance at light loads, Paper No. AIAA-2002-0787, in: 40th AIAA Aerospace Sciences Meeting and Exhibit, 14–17 January, Reno, NV, 2002.
- [12] J.A. Greenwood, The elastic stresses produced in the mid-plane of a slab by pressures applied symmetrically at its surface, in: *Proceedings of the Cambridge Philosophic Society*, 1964, pp. 159–169.
- [13] T.J. Lardner, Stresses in a thick plate with axially symmetric loading, *J. Appl. Mech.* (1965) 458–459.
- [14] C.W. Nelson, Further consideration of the thick-plate problem with axially symmetric loading, *J. Appl. Mech.* (1962) 91–98.
- [15] M.B.H. Mantelli, M.M. Yovanovich, Compact analytical model for overall thermal resistance of bolted joints, *Int. J. Heat Mass Transfer* 41 (10) (1998) 1255–1266.
- [16] K. Katwijk, J.K. Bennet, Thermal effects on structural design, in: *Proceedings of Spacecraft Thermal and Environmental Control Systems Symposium*, 1978.
- [17] ESA, *Spacecraft Thermal Control Handbook Data*, PSS-03-108, 1989.
- [18] J.P. Holman, *Experimental Methods for Engineers*, sixth ed., McGraw-Hill, Singapore, 1994, pp. 49–103.
- [19] M.R. Sridhar, M.M. Yovanovich, Review of elastic and plastic contact conductance models: comparison with experiment, *J. Thermophys. Heat Transfer* 8 (4) (1994) 633–640.
- [20] T.H. McWaid, Thermal contact resistance across pressed metal contact in a vacuum environment, Ph.D. Dissertation, University of California, Santa Barbara, CA, 1990.
- [21] Y.Z. Li, C.V. Madhusudana, E. Leonardi, On the enhancement of the thermal contact conductance: effect of loading history, *J. Heat Transfer* 122 (2000) 46–49.